

Partial wave analysis of $\psi(2S) \rightarrow p\bar{p}\eta$

M. Ablikim¹, M. N. Achasov⁶, O. Albayrak³, D. J. Ambrose³⁹, F. F. An¹, Q. An⁴⁰, J. Z. Bai¹, R. Baldini Ferroli^{17A}, Y. Ban²⁶, J. Becker², J. V. Bennett¹⁶, M. Bertani^{17A}, J. M. Bian³⁸, E. Boger^{19,a}, O. Bondarenko²⁰, I. Boyko¹⁹, R. A. Briere³, V. Bytev¹⁹, H. Cai⁴⁴, X. Cai¹, O. Cakir^{34A}, A. Calcaterra^{17A}, G. F. Cao¹, S. A. Cetin^{34B}, J. F. Chang¹, G. Chelkov^{19,a}, G. Chen¹, H. S. Chen¹, J. C. Chen¹, M. L. Chen¹, S. J. Chen²⁴, X. Chen²⁶, Y. B. Chen¹, H. P. Cheng¹⁴, Y. P. Chu¹, D. Cronin-Hennessy³⁸, H. L. Dai¹, J. P. Dai¹, D. Dedovich¹⁹, Z. Y. Deng¹, A. Denig¹⁸, I. Denysenko^{19,b}, M. Destefanis^{43A,43C}, W. M. Ding²⁸, Y. Ding²², L. Y. Dong¹, M. Y. Dong¹, S. X. Du⁴⁶, J. Fang¹, S. S. Fang¹, L. Fava^{43B,43C}, C. Q. Feng⁴⁰, P. Friedel², C. D. Fu¹, J. L. Fu²⁴, O. Fuks^{19,a}, Y. Gao³³, C. Geng⁴⁰, K. Goetzen⁷, W. X. Gong¹, W. Gradl¹⁸, M. Greco^{43A,43C}, M. H. Gu¹, Y. T. Gu⁹, Y. H. Guan³⁶, A. Q. Guo²⁵, L. B. Guo²³, T. Guo²³, Y. P. Guo²⁵, Y. L. Han¹, F. A. Harris³⁷, K. L. He¹, M. He¹, Z. Y. He²⁵, T. Held², Y. K. Heng¹, Z. L. Hou¹, C. Hu²³, H. M. Hu¹, J. F. Hu³⁵, T. Hu¹, G. M. Huang⁴, G. S. Huang⁴⁰, J. S. Huang¹², L. Huang¹, X. T. Huang²⁸, Y. Huang²⁴, Y. P. Huang¹, T. Hussain⁴², C. S. Ji⁴⁰, Q. Ji¹, Q. P. Ji²⁵, X. B. Ji¹, X. L. Ji¹, L. L. Jiang¹, X. S. Jiang¹, J. B. Jiao²⁸, Z. Jiao¹⁴, D. P. Jin¹, S. Jin¹, F. F. Jing³³, N. Kalantar-Nayestanaki²⁰, M. Kavatsyuk²⁰, B. Kopf², M. Kornicer³⁷, W. Kuehn³⁵, W. Lai¹, J. S. Lange³⁵, P. Larin¹¹, M. Leyhe², C. H. Li¹, Cheng Li⁴⁰, Cui Li⁴⁰, D. M. Li⁴⁶, F. Li¹, G. Li¹, H. B. Li¹, J. C. Li¹, K. Li¹⁰, Lei Li¹, Q. J. Li¹, S. L. Li¹, W. D. Li¹, W. G. Li¹, X. L. Li²⁸, X. N. Li¹, X. Q. Li²⁵, X. R. Li²⁷, Z. B. Li³², H. Liang⁴⁰, Y. F. Liang³⁰, Y. T. Liang³⁵, G. R. Liao³³, X. T. Liao¹, D. Lin¹¹, B. J. Liu¹, C. L. Liu³, C. X. Liu¹, F. H. Liu²⁹, Fang Liu¹, Feng Liu⁴, H. Liu¹, H. B. Liu⁹, H. H. Liu¹³, H. M. Liu¹, H. W. Liu¹, J. P. Liu⁴⁴, K. Liu³³, K. Y. Liu²², Kai Liu³⁶, P. L. Liu²⁸, Q. Liu³⁶, S. B. Liu⁴⁰, X. Liu²¹, Y. B. Liu²⁵, Z. A. Liu¹, Zhiqiang Liu¹, Zhiqing Liu¹, H. Loehner²⁰, G. R. Lu¹², H. J. Lu¹⁴, J. G. Lu¹, Q. W. Lu²⁹, X. R. Lu³⁶, Y. P. Lu¹, C. L. Luo²³, M. X. Luo⁴⁵, T. Luo³⁷, X. L. Luo¹, M. Lv¹, C. L. Ma³⁶, F. C. Ma²², H. L. Ma¹, Q. M. Ma¹, S. Ma¹, T. Ma¹, X. Y. Ma¹, F. E. Maas¹¹, M. Maggiora^{43A,43C}, Q. A. Malik⁴², Y. J. Mao²⁶, Z. P. Mao¹, J. G. Messchendorp²⁰, J. Min¹, T. J. Min¹, R. E. Mitchell¹⁶, X. H. Mo¹, H. Moeini²⁰, C. Morales Morales¹¹, K. Moriya¹⁶, N. Yu. Muchnoi⁶, H. Muramatsu³⁹, Y. Nefedov¹⁹, C. Nicholson³⁶, I. B. Nikolaev⁶, Z. Ning¹, S. L. Olsen²⁷, Q. Ouyang¹, S. Pacetti^{17B}, J. W. Park²⁷, M. Pelizaeus², H. P. Peng⁴⁰, K. Peters⁷, J. L. Ping²³, R. G. Ping¹, R. Poling³⁸, E. Prencipe¹⁸, M. Qi²⁴, S. Qian¹, C. F. Qiao³⁶, L. Q. Qin²⁸, X. S. Qin¹, Y. Qin²⁶, Z. H. Qin¹, J. F. Qiu¹, K. H. Rashid⁴², G. Rong¹, X. D. Ruan⁹, A. Sarantsev^{19,c}, B. D. Schaefer¹⁶, M. Shao⁴⁰, C. P. Shen^{37,d}, X. Y. Shen¹, H. Y. Sheng¹, M. R. Shepherd¹⁶, W. M. Song¹, X. Y. Song¹, S. Spataro^{43A,43C}, B. Spruck³⁵, D. H. Sun¹, G. X. Sun¹, J. F. Sun¹², S. S. Sun¹, Y. J. Sun⁴⁰, Y. Z. Sun¹, Z. J. Sun¹, Z. T. Sun⁴⁰, C. J. Tang³⁰, X. Tang¹, I. Tapan^{34C}, E. H. Thorndike³⁹, H. L. Tian¹, D. Toth³⁸, M. Ullrich³⁵, I. Uman^{34B}, G. S. Varner³⁷, B. Q. Wang²⁶, D. Wang²⁶, D. Y. Wang²⁶, J. X. Wang¹, K. Wang¹, L. L. Wang¹, L. S. Wang¹, M. Wang²⁸, P. Wang¹, P. L. Wang¹, Q. J. Wang¹, S. G. Wang²⁶, X. F. Wang³³, X. L. Wang⁴⁰, Y. D. Wang^{17A}, Y. F. Wang⁴⁰, S. P. Wen¹, M. Werner³⁵, U. Wiedner², L. H. Wu¹, N. Wu¹, S. X. Wu⁴⁰, W. Wu²⁵, Z. Wu¹, L. G. Xia³³, Y. X. Xia¹⁵, Z. J. Xiao²³, Y. G. Xie¹, Q. L. Xiu¹, G. F. Xu¹, G. M. Xu²⁶, Q. J. Xu¹⁰, Q. N. Xu³⁶, X. P. Xu³¹, Z. R. Xu⁴⁰, F. Xue⁴, Z. Xue¹, L. Yan⁴⁰, W. B. Yan⁴⁰, Y. H. Yan¹⁵, H. X. Yang¹, Y. Yang⁴, Y. X. Yang⁸, H. Ye¹, M. Ye¹, M. H. Ye⁵, B. X. Yu¹, C. X. Yu²⁵, H. W. Yu²⁶, J. S. Yu²¹, S. P. Yu²⁸, C. Z. Yuan¹, Y. Yuan¹, A. A. Zafar⁴², A. Zallo^{17A}, S. L. Zang²⁴, Y. Zeng¹⁵, B. X. Zhang¹, B. Y. Zhang¹, C. Zhang²⁴, C. C. Zhang¹, D. H. Zhang¹, H. H. Zhang³², H. Y. Zhang¹, J. Q. Zhang¹, J. W. Zhang¹, J. Y. Zhang¹, J. Z. Zhang¹, LiLi Zhang¹⁵, R. Zhang³⁶, S. H. Zhang¹, X. J. Zhang¹, X. Y. Zhang²⁸, Y. Zhang¹, Y. H. Zhang¹, Z. P. Zhang⁴⁰, Z. Y. Zhang⁴⁴, Zhenghao Zhang⁴, G. Zhao¹, H. S. Zhao¹, J. W. Zhao¹, K. X. Zhao²³, Lei Zhao⁴⁰, Ling Zhao¹, M. G. Zhao²⁵, Q. Zhao¹, S. J. Zhao⁴⁶, T. C. Zhao¹, X. H. Zhao²⁴, Y. B. Zhao¹, Z. G. Zhao⁴⁰, A. Zhemchugov^{19,a}, B. Zheng⁴¹, J. P. Zheng¹, Y. H. Zheng³⁶, B. Zhong²³, L. Zhou¹, X. Zhou⁴⁴, X. K. Zhou³⁶, X. R. Zhou⁴⁰, C. Zhu¹, K. Zhu¹, K. J. Zhu¹, S. H. Zhu¹, X. L. Zhu³³, Y. C. Zhu⁴⁰, Y. M. Zhu²⁵, Y. S. Zhu¹, Z. A. Zhu¹, J. Zhuang¹, B. S. Zou¹, J. H. Zou¹

(BESIII Collaboration)

¹ Institute of High Energy Physics, Beijing 100049, People's Republic of China

² Bochum Ruhr-University, D-44780 Bochum, Germany

³ Carnegie Mellon University, Pittsburgh, Pennsylvania 15213, USA

⁴ Central China Normal University, Wuhan 430079, People's Republic of China

⁵ China Center of Advanced Science and Technology, Beijing 100190, People's Republic of China

⁶ G.I. Budker Institute of Nuclear Physics SB RAS (BINP), Novosibirsk 630090, Russia

⁷ GSI Helmholtzcentre for Heavy Ion Research GmbH, D-64291 Darmstadt, Germany

⁸ Guangxi Normal University, Guilin 541004, People's Republic of China

⁹ GuangXi University, Nanning 530004, People's Republic of China

¹⁰ Hangzhou Normal University, Hangzhou 310036, People's Republic of China

¹¹ Helmholtz Institute Mainz, Johann-Joachim-Becher-Weg 45, D-55099 Mainz, Germany

¹² Henan Normal University, Xinxiang 453007, People's Republic of China

¹³ Henan University of Science and Technology, Luoyang 471003, People's Republic of China

¹⁴ Huangshan College, Huangshan 245000, People's Republic of China

¹⁵ Hunan University, Changsha 410082, People's Republic of China

¹⁶ Indiana University, Bloomington, Indiana 47405, USA

¹⁷ (A)INFN Laboratori Nazionali di Frascati, I-00044, Frascati, Italy; (B)INFN and University of Perugia, I-06100, Perugia, Italy

¹⁸ Johannes Gutenberg University of Mainz, Johann-Joachim-Becher-Weg 45, D-55099 Mainz, Germany

- ¹⁹ Joint Institute for Nuclear Research, 141980 Dubna, Moscow region, Russia
- ²⁰ KVI, University of Groningen, NL-9747 AA Groningen, The Netherlands
- ²¹ Lanzhou University, Lanzhou 730000, People's Republic of China
- ²² Liaoning University, Shenyang 110036, People's Republic of China
- ²³ Nanjing Normal University, Nanjing 210023, People's Republic of China
- ²⁴ Nanjing University, Nanjing 210093, People's Republic of China
- ²⁵ Nankai University, Tianjin 300071, People's Republic of China
- ²⁶ Peking University, Beijing 100871, People's Republic of China
- ²⁷ Seoul National University, Seoul, 151-747 Korea
- ²⁸ Shandong University, Jinan 250100, People's Republic of China
- ²⁹ Shanxi University, Taiyuan 030006, People's Republic of China
- ³⁰ Sichuan University, Chengdu 610064, People's Republic of China
- ³¹ Soochow University, Suzhou 215006, People's Republic of China
- ³² Sun Yat-Sen University, Guangzhou 510275, People's Republic of China
- ³³ Tsinghua University, Beijing 100084, People's Republic of China
- ³⁴ (A)Ankara University, Dogol Caddesi, 06100 Tandogan, Ankara, Turkey; (B)Dogus University, 34722 Istanbul, Turkey; (C)Uludag University, 16059 Bursa, Turkey
- ³⁵ Universitaet Giessen, D-35392 Giessen, Germany
- ³⁶ University of Chinese Academy of Sciences, Beijing 100049, People's Republic of China
- ³⁷ University of Hawaii, Honolulu, Hawaii 96822, USA
- ³⁸ University of Minnesota, Minneapolis, Minnesota 55455, USA
- ³⁹ University of Rochester, Rochester, New York 14627, USA
- ⁴⁰ University of Science and Technology of China, Hefei 230026, People's Republic of China
- ⁴¹ University of South China, Hengyang 421001, People's Republic of China
- ⁴² University of the Punjab, Lahore-54590, Pakistan
- ⁴³ (A)University of Turin, I-10125, Turin, Italy; (B)University of Eastern Piedmont, I-15121, Alessandria, Italy; (C)INFN, I-10125, Turin, Italy
- ⁴⁴ Wuhan University, Wuhan 430072, People's Republic of China
- ⁴⁵ Zhejiang University, Hangzhou 310027, People's Republic of China
- ⁴⁶ Zhengzhou University, Zhengzhou 450001, People's Republic of China
- ^a Also at the Moscow Institute of Physics and Technology, Moscow 141700, Russia
- ^b On leave from the Bogolyubov Institute for Theoretical Physics, Kiev 03680, Ukraine
- ^c Also at the PNPI, Gatchina 188300, Russia
- ^d Present address: Nagoya University, Nagoya 464-8601, Japan

Using a sample of 1.06×10^8 $\psi(2S)$ events collected with the BESIII detector at BEPCII, the decay $\psi(2S) \rightarrow p\bar{p}\eta$ is studied. A partial wave analysis determines that the intermediate state $N(1535)$ with a mass of $1524 \pm 5_{-4}^{+10}$ MeV/ c^2 and a width of 130_{-24-10}^{+27+57} MeV/ c^2 is dominant in the decay; the product branching fraction is determined to be $B(\psi(2S) \rightarrow N(1535)\bar{p}) \times B(N(1535) \rightarrow p\eta) + c.c. = (5.2 \pm 0.3_{-1.2}^{+3.2}) \times 10^{-5}$. Furthermore, the branching fraction of $\psi(2S) \rightarrow \eta p\bar{p}$ is measured to be $(6.4 \pm 0.2 \pm 0.6) \times 10^{-5}$.

PACS numbers: 13.25.Gv, 12.38.Qk, 14.20.Gk, 14.40.Cs

I. INTRODUCTION

Baryon spectroscopy is an important field to understand the internal structure of hadrons. Within the static quark model, the baryon octet and decuplet are well described. About half a century after the introduction of the quark model, however, a substantial number of light baryons predicted by the quark model have not been observed experimentally, which is known as the "missing baryon problem" [1, 2]. One possibility could be that the missing states simply do not exist, which has led to the development of new phenomenological models, eg. the di-quark model [3]. Alternatively, the coupling of the unobserved states through conventional production channels could be small, which makes their observation more difficult.

In addition to fixed target experiments [4–11],

charmonium decays produced in e^+e^- collisions open a window to hunt for the missing baryons [12]. The Beijing Spectrometer (BES) [13] experiment started a baryon program about a decade ago with the study of $N(1535)$ and $N(1650)$ in $J/\psi \rightarrow p\bar{p}\eta$ by partial wave analysis (PWA) [14] using a sample of 7.8 million J/ψ events. Using 58 million J/ψ events collected at the BESII detector, a new excited nucleon $N(2065)$ [15, 16] was observed in $J/\psi \rightarrow p\bar{n}\pi^-$ [17] and subsequently confirmed in $J/\psi \rightarrow p\bar{p}\pi^0$ [18]. BESII also studied $\psi(2S) \rightarrow p\bar{p}\gamma\gamma$, where both $p\bar{p}\pi^0$ and $p\bar{p}\eta$ were observed, $\psi(2S) \rightarrow p\bar{p}\eta$ for the first time with a branching fraction of $(5.8 \pm 1.1 \pm 0.7) \times 10^{-5}$. In both decays, there was weak evidence for a $p\bar{p}$ threshold mass enhancement but no PWA was performed [19]. Most recently BESIII reported PWA results of $\psi(2S) \rightarrow p\bar{p}\pi^0$ [20], and two new broad excited nucleons, $N(2300)$ and $N(2570)$, were observed.

However, no clear evidence for $N(2065)$ was found. Using 24.5×10^6 $\psi(2S)$ events, CLEO-c [21] reported the analysis of $\psi(2S) \rightarrow \gamma p\bar{p}, \pi^0 p\bar{p}$ and $\eta p\bar{p}$ without considering interference effects, in which $N(1535)$ and a $p\bar{p}$ enhancement ($R_1(2100)$) were investigated in $\psi(2S)$ decay to $p\bar{p}\eta$. Those results show that J/ψ and $\psi(2S)$ decays offer a unique place to study baryon spectroscopy.

In this paper, using the 106 million $\psi(2S)$ events taken at the BESIII detector, a full PWA of the decay $\psi(2S) \rightarrow p\bar{p}\eta$ is performed.

II. BESIII DETECTOR AND MONTE CARLO SIMULATION

BEPCII [22] is a double-ring e^+e^- collider designed to provide a peak luminosity of $10^{33} \text{ cm}^{-2}\text{s}^{-1}$ at a beam current of 0.93 A. The BESIII [22] detector has a geometrical acceptance of 93% of 4π and consists of four main components: (1) A small-cell, helium-based (40% He, 60% C_3H_8) Main Drift Chamber (MDC) with 43 layers providing an average single-hit resolution of $135 \mu\text{m}$, charged-particle momentum resolution in a 1 T magnetic field of 0.5% at $1 \text{ GeV}/c^2$, and a dE/dx resolution, which is better than 6%. (2) A Time-Of-Flight system (TOF) constructed of 5-cm-thick plastic scintillators, with 176 detectors of 2.4 m length in two layers in the barrel and 96 fan-shaped detectors in the endcaps. The barrel (endcap) time resolution of 80 ps (110 ps) provides 2σ K/π separation for momenta up to $\sim 1.0 \text{ GeV}/c^2$. (3) An ElectroMagnetic Calorimeter (EMC) consisting of 6240 CsI(Tl) crystals in a cylindrical structure (barrel) and two endcaps. The energy resolution at 1.0 GeV is 2.5% (5%) in the barrel (endcaps), and the position resolution in the barrel (endcaps) is 6 mm (9 mm). (4) The MUon Counter (MUC) consists of 1000 m^2 of Resistive Plate Chambers (RPCs) in nine barrel and eight endcap layers and provides 2 cm position resolution.

A GEANT4-based simulation software BOOST [23] includes the geometric and material description of the BESIII detectors, the detector response and digitization models, as well as the tracking of the detector running conditions and performance. The production of the $\psi(2S)$ resonance is simulated by the Monte Carlo (MC) event generator KKMC [24], while the decays are generated by EvtGen [25] for known decay modes with branching ratios being set to the PDG [26] world average values, and by Lundcharm [27] for the remaining unknown decays. The analysis is performed in the framework of the BESIII Offline Software System (BOSS) [28] which takes care of the detector calibration, event reconstruction and data storage.

III. EVENT SELECTION

For $\psi(2S) \rightarrow p\bar{p}\eta$ ($\eta \rightarrow \gamma\gamma$), the topology is quite simple, $p\bar{p}\gamma\gamma$. Each candidate event is required to have two good charged tracks reconstructed from the MDC with total charge zero. The point of closest approach to the beamline of each charged track is required to be within ± 20 cm in the beam direction and 2 cm in the plane perpendicular to the beam. Both tracks must have the polar angle θ in the range of $|\cos\theta| < 0.93$. The TOF and the specific energy loss dE/dx of a particle measured in the MDC are combined to calculate particle identification (PID) probabilities for pion, kaon and proton hypotheses. The particle type with the highest probability is assigned to each track. In this analysis, one charged track is required to be identified as a proton and the other as an anti-proton.

Photon candidates are reconstructed by clustering EMC crystal energies. For each photon, the minimum energy is 25 MeV for barrel showers ($|\cos\theta| < 0.80$) and 50 MeV for endcap showers ($0.86 < |\cos\theta| < 0.92$). To exclude showers from charged particles, the angle between the nearest proton track and the shower must be greater than 10° , while for the anti-proton the angle has to be greater than 30° . Timing requirements are used to suppress electronic noise and energy deposits in the EMC unrelated to the event. At least two good photons are required.

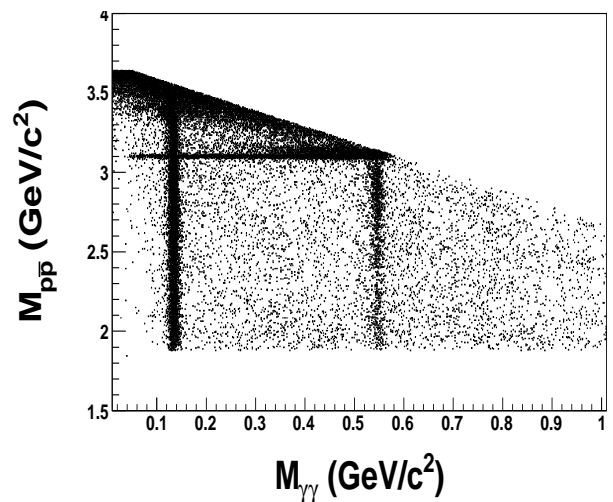


FIG. 1: Scatter plots of $p\bar{p}$ invariant mass versus $\gamma\gamma$ invariant mass

For the candidates remaining, a four-constraint kinematic fit imposing energy-momentum conservation is made under the $p\bar{p}\gamma\gamma$ hypothesis. If the number of selected photons is greater than two, the fit is repeated using all permutations of photons. The two photon combination with the minimum fit $\chi^2_{p\bar{p}\gamma\gamma}$ is selected, and $\chi^2_{p\bar{p}\gamma\gamma}$ is required to be less than 20. Because data and MC simulation do not agree well in the low momentum region, the momenta of the proton and anti-proton are

required to be greater than 300 MeV/c. Figure 1 shows the scatter plot of $M_{p\bar{p}}$ versus $M_{\gamma\gamma}$ for events satisfying the above requirements, where the two vertical bands correspond to the decays $\psi(2S) \rightarrow p\bar{p}\pi^0$ and $\psi(2S) \rightarrow p\bar{p}\eta$, and the horizontal band corresponds to the decay $\psi(2S) \rightarrow X + J/\psi$ ($J/\psi \rightarrow p\bar{p}$). To remove the background events from $\psi(2S) \rightarrow \eta J/\psi$ and $\psi(2S) \rightarrow \gamma\chi_{cJ}$, $M_{p\bar{p}} < 3.067 \text{ GeV}/c^2$ and $M_{p\bar{p}} < (3.4 \text{ GeV}/c^2 - 0.75 \times M_{\gamma\gamma})$ are required. To select a clean sample, $M_{\gamma\gamma}$ is required to be in the η mass region, $|M_{\gamma\gamma} - M_\eta| < 21 \text{ MeV}/c^2$.

After the above event selection, 745 candidate events are selected. The Dalitz plot of $M_{p\eta}$ versus $M_{\bar{p}\eta}$ is shown in Fig. 2 (a), where two clusters, corresponding to the $p\eta$ mass threshold enhancement displayed in Fig. 2 (b) and Fig. 2 (c) are visible. Both the mass spectra and the Dalitz plot display an asymmetry for $p\eta$ and $\bar{p}\eta$, which is mainly caused by different detection efficiencies for the proton and anti-proton.

To investigate possible background events, the same analysis is performed on the MC sample of 100 million inclusive $\psi(2S)$ events, and 11 background events are found from the channels, $\psi(2S) \rightarrow \gamma\chi_{cJ}(\chi_{cJ} \rightarrow p\bar{p}\pi^0)$, $\psi(2S) \rightarrow \gamma\chi_{cJ}(\chi_{cJ} \rightarrow \gamma J/\psi, J/\psi \rightarrow \gamma p\bar{p})$ and $\psi(2S) \rightarrow \gamma\chi_{c0}(\chi_{c0} \rightarrow \bar{p}\Delta^+, \Delta^+ \rightarrow p\pi^0)$, which is compatible with the number of background events, 14, estimated with η sidebands ($|M_{\gamma\gamma} - 0.43| < 50 \text{ MeV}/c^2$ and $|M_{\gamma\gamma} - 0.65| < 50 \text{ MeV}/c^2$). Additionally, 42.6 pb^{-1} of continuum data taken at $3.65 \text{ GeV}/c^2$ is used for an estimation of the background from QED processes and 51 background events are obtained after normalization with the luminosity of the continuum data and $\psi(2S)$ data. The background events from η sidebands and the continuum data will be considered in the PWA of $\psi(2S) \rightarrow p\bar{p}\eta$.

IV. PARTIAL WAVE ANALYSIS

The two-body decay amplitudes in the sequential decay process $\psi(2S) \rightarrow N^*\bar{p}, N^* \rightarrow \eta p$ (the charge-conjugate reaction is always implied unless explicitly mentioned) are constructed using the relativistic covariant tensor amplitude formalism [29], and the maximum likelihood method is used in the PWA [18]. In $\psi(2S) \rightarrow N_X\bar{p}, N_X \rightarrow \eta p$, A_j is described as

$$A_j = A_{prod-X}^j(BW)_X A_{decay-X}, \quad (1)$$

where A_{prod-X}^j is the amplitude, describing the production of the intermediate resonance N_X , BW_X is the Breit-Weigner propagator of N_X , and $A_{decay-X}$ is the decay amplitude of N_X . The total differential cross section $\frac{d\sigma}{d\Phi}$ is

$$\frac{d\sigma}{d\Phi} = \left| \sum_j c_j A_j + F_{phsp} \right|^2, \quad (2)$$

where F_{phsp} denotes the non-resonant contribution described by a interfering phase space term. The probability to observe the event characterized by the measurement ξ is

$$P(\xi) = \frac{\omega(\xi)\epsilon(\xi)}{\int d\xi\omega(\xi)\epsilon(\xi)}, \quad (3)$$

where $\omega(\xi) \equiv \frac{d\sigma}{d\Phi}$ and $\epsilon(\xi)$ is the detection efficiency. $\int d\xi\omega(\xi)\epsilon(\xi)$ is the normalization integral calculated from the exclusive Monte Carlo sample. The joint probability density for observing n events in the data sample is

$$\mathcal{L} = P(\xi_1, \xi_2, \dots, \xi_n) = \prod_{i=1}^n P(\xi_i) = \prod_{i=1}^n \frac{\omega(\xi_i)\epsilon(\xi_i)}{\int d\xi\omega(\xi)\epsilon(\xi)}, \quad (4)$$

Rather than maximizing the likelihood function $\ln(\mathcal{L})$, $S = -\ln\mathcal{L}$ is minimized to obtain c_j parameters, as well as the masses and widths of the resonances

$$-\ln\mathcal{L} = -\sum_{i=1}^n \ln\left(\frac{\omega(\xi_i)}{\int d\xi\omega(\xi)\epsilon(\xi)}\right) - \sum_{i=1}^n \ln\epsilon(\xi_i), \quad (5)$$

For a given data set, the second term is a constant and has no impact on the determination of the parameters of the amplitudes or on the relative changes of S values. So, for the fitting, $-\ln\mathcal{L}$ is defined as

$$-\ln\mathcal{L} \equiv -\sum_{i=1}^n \ln\left(\frac{\omega(\xi_i)}{\int d\xi\omega(\xi)\epsilon(\xi)}\right), \quad (6)$$

The contribution of non- η events and QED processes can be estimated with η sidebands and continuum data. In the log-likelihood calculation, the likelihood value of η sidebands and continuum data events are given negative weights, and are removed from data, since the log-likelihood value of data is the sum of the log-likelihood values of signal and background events

$$S = -[(-\ln(\mathcal{L}))_{data} - (-\ln(\mathcal{L}))_{bg}] \quad (7)$$

The free parameters are optimized by FUMILI [30]. In the minimization procedure, a change in log-likelihood of 0.5 represents one standard deviation for each parameter.

In the analysis, the following two Breit-Wigner formulas are used to describe the resonance. One form has a width which is independent of the energy of the intermediate state

$$BW(s) = \frac{1}{M_{N^*}^2 - s - iM_{N^*}\Gamma_{N^*}}, \quad (8)$$

where s is the invariant mass-squared. For $N(1535)$ with its mass close to the threshold of its dominant decay

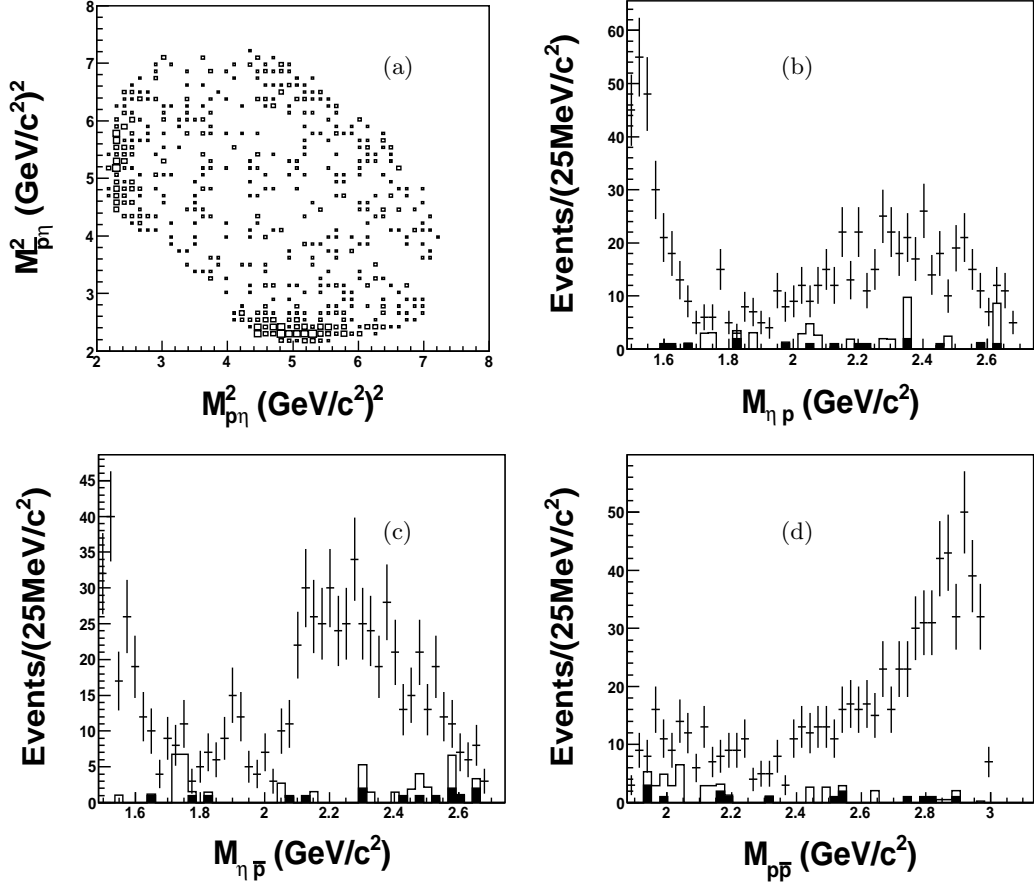


FIG. 2: (a) The Dalitz plot of $\psi(2S) \rightarrow \eta p \bar{p}$ and distributions for (b) $M_{\eta p}$, (c) $M_{\eta \bar{p}}$, and (d) $M_{p \bar{p}}$. The crosses represent the data, the blank histograms show background events from continuum data, and the shaded histograms represent the background events from η sidebands.

channel $N\eta$, the approximation of a constant width is not very good. Thus a phase space dependent width for $N(1535)$ is also used

$$BW(s) = \frac{1}{M_{N^*}^2 - s - iM_{N^*}\Gamma_{N^*}(s)}. \quad (9)$$

The phase space dependent widths can be written as [31]

$$\Gamma_{N^*}(s) = \Gamma_{N^*}^0 \left(0.5 \frac{\rho_{\pi N}(s)}{\rho_{\pi N}(M_{N^*}^2)} + 0.5 \frac{\rho_{\eta N}(s)}{\rho_{\eta N}(M_{N^*}^2)} \right), \quad (10)$$

where $\rho_{\pi N}$ and $\rho_{\eta N}$ are the phase space factors for πN and ηN final states, respectively,

$$\begin{aligned} \rho_{XN}(s) &= \frac{2q_{XN}(s)}{\sqrt{s}} \\ &= \frac{\sqrt{(s - (M_N + M_X)^2)(s - (M_N - M_X)^2)}}{s}, \end{aligned} \quad (11)$$

where X is π or η , and $q_{XN}(s)$ is the momentum of X in the center-of-mass system of XN .

V. SYSTEMATIC ERRORS

The systematic error sources and their corresponding contributions to the measurement of mass, width and branching fractions are discussed below.

- To investigate the impact on the PWA results from other possible components, the analysis is also performed including other possible N^* states (eg. $N(1520)$, $N(1650)$, $N(1700)$, $N(1710)$, $N(1720)$, $N(1895)$ and $N(1900)$); the changes of the mass, width, and observed number of $N(1535) \rightarrow p\eta$ events are taken as the systematic errors by summing them in quadrature.
- In the analysis, the background level is quite low, and the events from η sidebands and continuum data are considered in the PWA. To estimate the uncertainty, the background events from η sidebands are varied by $\pm 50\%$, and the biggest change of the results is assigned as the systematic error.
- In Eq. (10), the weight of the phase space factors for both ηN and πN is set to be 0.5. The change

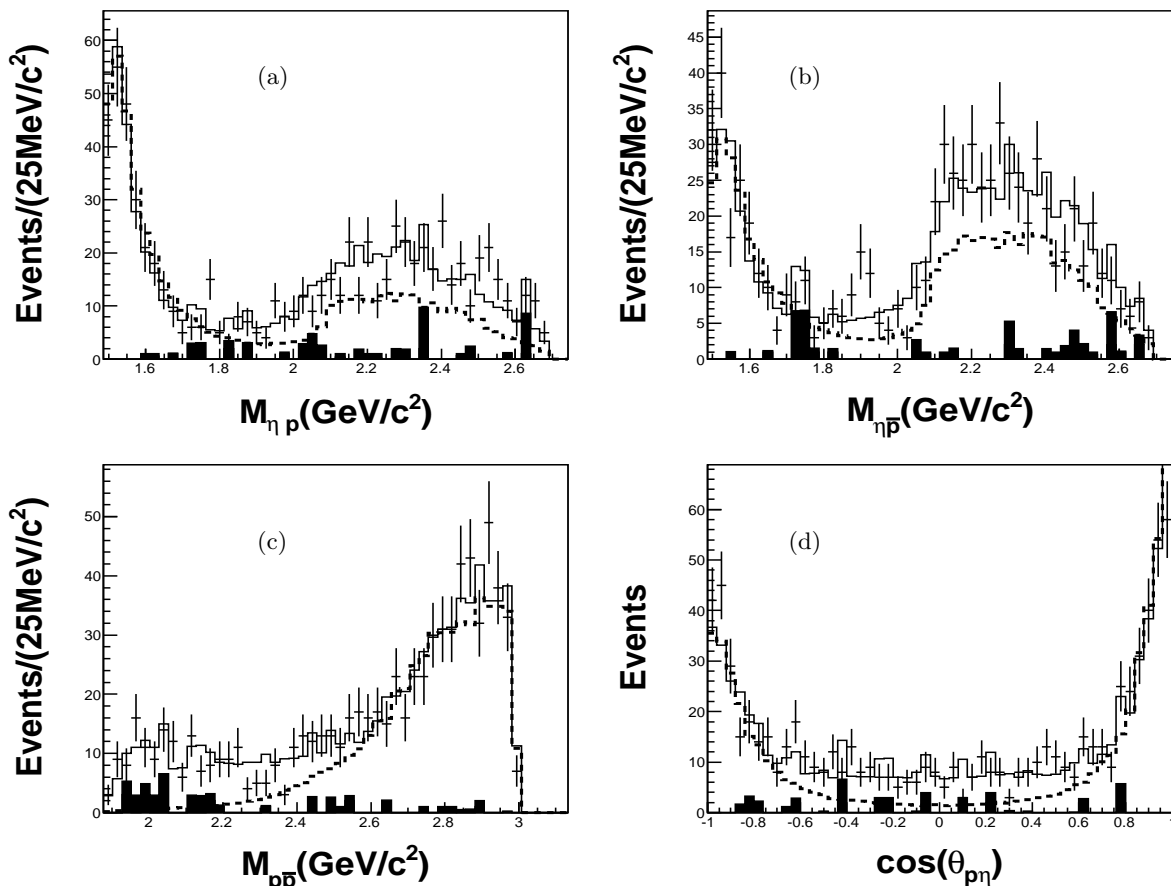


FIG. 3: Distributions of (a) $M_{p\eta}$, (b) $M_{\bar{p}\eta}$, (c) $M_{p\bar{p}}$ and (d) the angle between $p\eta$ in the $p\bar{p}$ system. The crosses are for data, the blank histograms for PWA projections, the dashed lines for the contribution of $N(1535)$ and the shaded histograms for the background events from η sidebands and continuum data.

of the results due to the variation of the weights in the range of $0 \sim 1$ is taken as the systematic error.

- The MDC tracking efficiency was studied with the clean sample of $J/\psi \rightarrow p\bar{p}\pi^+\pi^-$ events, as described in Ref [32]. The difference between data and MC is less than 2% per charged track. Here, 4% is taken as systematic error for the proton and anti-proton.
- According to the particle identification efficiency study in Ref [32], the difference of the particle identification efficiencies between MC simulation and data is around 2% for each charged track. In this study, the two charged tracks are required to be identified as p and \bar{p} , so 4% is taken as its systematic error from this source.
- The systematic error from the photon detection efficiency has been studied using $J/\psi \rightarrow \rho^0\pi^0$ events in Ref. [33]. The result indicates that the difference between data and MC simulation is about 1% for each photon. For the decay mode analyzed in this paper, 2% is taken as systematic error from two photons in the final states.

- In order to estimate the systematic error of the kinematic fit, a clean sample of $J/\psi \rightarrow p\bar{p}\pi^0$ is selected. The difference of the efficiency between data and MC with and without using the four constraint kinematic fit, 7%, is taken as the systematic error.
- The number of $\psi(2S)$ events, $(1.06 \pm 0.86) \times 10^8$ [34], was determined from inclusive hadrons, and the systematic uncertainty is 0.82%.

Table I summarizes the systematic error contributions from different sources for the measurements of mass, width and branching fractions, and the total is the sum of them in quadrature.

VI. RESULTS

The PWA results, including the invariant mass spectra of $p\bar{p}$, ηp , $\eta\bar{p}$ and angular distributions, are shown as histograms in Fig. 3 and are consistent with the data. The best solution indicates that $N(1535)$ combined with an interfering phase space is sufficient to describe the data. We observe 527 ± 27 $N(1535) \rightarrow p\eta$ events

TABLE I: Summary of the systematic error contributions from different sources.

Source	$\Delta M(\text{MeV}/c^2)$	$\Delta \Gamma(\text{MeV}/c^2)$	$\Delta B(\%)$
Additional Resonances	+2 -4	+56 -0	+59 -6
Different BW Formula	—	—	+17 -21
Background Uncertainty	+10	+10 -10	+8
MDC Tracking	—	—	± 4
Photon Detection	—	—	± 2
Particle ID	—	—	± 4
Kinematic Fit	—	—	± 7
The number of $\psi(2S)$ events	—	—	± 0.82
Total	+10 -4	+57 -10	+63 -23

with a mass $M = (1524 \pm 5_{-4}^{+10}) \text{ MeV}/c^2$, a width $\Gamma = 130_{-24}^{+27+57} \text{ MeV}/c^2$, and a statistical significance larger than 10σ . Here, the first error is statistical and the second is systematic. The contributions of $N(1535)$ and phase space are 70.8% and 61.0%. To determine the detection efficiency of $\psi(2S) \rightarrow N(1535)\bar{p}$, the MC events are generated in accordance with the PWA amplitudes for $\psi(2S) \rightarrow N(1535)\bar{p}$. With the detection efficiency of 24.1%, the product branching fraction of $\psi(2S) \rightarrow N(1535)\bar{p}$ ($N(1535) \rightarrow p\eta$) is calculated to be

$$B(\psi(2S) \rightarrow N(1535)\bar{p} (N(1535) \rightarrow p\eta)) = \frac{N_{obs}}{\varepsilon \cdot N_{\psi(2S)} \cdot B(\eta \rightarrow \gamma\gamma)} = (5.2 \pm 0.3_{-1.2}^{+3.2}) \times 10^{-5}, \quad (12)$$

where the number of $\psi(2S)$ events, $N_{\psi(2S)}$, is $(1.06 \pm 0.86) \times 10^8$ determined from $\psi(2S)$ inclusive decays [34]; $B(\eta \rightarrow \gamma\gamma)$ is the world average value [35], and the first error is statistical and the second systematic.

To investigate the $p\bar{p}$ mass enhancement observed at BESII [19] and CLEO-c [21], which did not use a PWA, a scan for an additional 1^{--} resonance described by a Breit-Wigner function is performed. The widths used are 50 MeV/c^2 , 100 MeV/c^2 , 200 MeV/c^2 , 300 MeV/c^2 , 400 MeV/c^2 , 500 MeV/c^2 and 600 MeV/c^2 . The mass is allowed to vary from 1900 MeV/c^2 to 3000 MeV/c^2 with steps of 2 MeV/c^2 . There is no evidence for a $p\bar{p}$ resonance in this region, indicating that the threshold enhancement can be explained by interference between the $N(1535)$ and phase space.

Subtracting the 51 and 15 background events from QED processes and from η sidebands, respectively, the number of $\psi(2S) \rightarrow p\bar{p}\eta$ events is calculated to be 679 ± 26 . In addition to the contribution from $N(1535)$, the contribution from the phase space events is taken into account in the determination of the detection efficiency according to the PWA results. With the detection efficiency of 25.6%, the branching fraction of $\psi(2S) \rightarrow$

$p\bar{p}\eta$ is measured to be

$$B(\psi(2S) \rightarrow \eta p\bar{p}) = (6.4 \pm 0.2 \pm 0.6) \times 10^{-5} \quad (13)$$

VII. SUMMARY

Based on 1.06×10^8 $\psi(2S)$ events collected with BESIII detector, a full PWA on the 745 $\psi(2S) \rightarrow p\bar{p}\eta$ candidates is performed, and the results indicate that the dominant contribution is from $\psi(2S) \rightarrow N(1535)\bar{p}$. The mass and width of $N(1535)$ are determined to be $1524 \pm 5_{-4}^{+10} \text{ MeV}/c^2$ and $130_{-24}^{+27+57} \text{ MeV}/c^2$, respectively, which are consistent with those from previous measurements listed in the PDG [35]. The product of the branching fractions is calculated to be $B(\psi(2S) \rightarrow N(1535)\bar{p}) \times B(N(1535) \rightarrow p\eta) + c.c. = (5.2 \pm 0.3_{-1.2}^{+3.2}) \times 10^{-5}$. The $p\bar{p}$ mass enhancement observed by BESII is investigated, and the statistical significance of an additional $p\bar{p}$ resonance is less than 3σ .

The branching fraction of $\psi(2S) \rightarrow \eta p\bar{p}$ is determined to be $(6.4 \pm 0.2 \pm 0.6) \times 10^{-5}$, where the detection efficiency is determined from MC simulation events generated based on the PWA results. Compared with the branching fraction of $J/\psi \rightarrow p\bar{p}\eta$ [35],

$$Q_{p\bar{p}\eta} = \frac{B(\psi(2S) \rightarrow \eta p\bar{p})}{B(J/\psi \rightarrow \eta p\bar{p})} = (3.2 \pm 0.4)\%, \quad (14)$$

which improves the BESII measurement [19] of $(2.8 \pm 0.7)\%$, and indicates that the decay $\psi(2S) \rightarrow p\bar{p}\eta$ is suppressed compared with the "12% rule".

VIII. ACKNOWLEDGMENTS

The BESIII collaboration thanks the staff of BEPCII and the computing center for their hard efforts. This work is supported in part by the Ministry of Science and

Technology of China under Contract No. 2009CB825200; National Natural Science Foundation of China (NSFC) under Contracts Nos. 10625524, 10821063, 10825524, 10835001, 10935007, 11125525, 11235011, 10805053; Joint Funds of the National Natural Science Foundation of China under Contracts Nos. 11079008, 11179007; the Chinese Academy of Sciences (CAS) Large-Scale Scientific Facility Program; CAS under Contracts Nos. KJCX2-YW-N29, KJCX2-YW-N45; 100 Talents Program of CAS; German Research Foundation DFG under Contract No. Collaborative Research Center

CRC-1044; Istituto Nazionale di Fisica Nucleare, Italy; Ministry of Development of Turkey under Contract No. DPT2006K-120470; U. S. Department of Energy under Contracts Nos. DE-FG02-04ER41291, DE-FG02-05ER41374, DE-FG02-94ER40823; U.S. National Science Foundation; University of Groningen (RuG) and the Helmholtzzentrum fuer Schwerionenforschung GmbH (GSI), Darmstadt; WCU Program of National Research Foundation of Korea under Contract No. R32-2008-000-10155-0

-
- [1] S. Capstick and W. Roberts, Phys. Rev. D **47**, 1994 (1993).
- [2] N. Isgur and G. Karl, Phys. Rev. D **19**, 2653 (1979).
- [3] M. Oettel, G. Hellstern, R. Alkofer, and H. Reinhardt, Phys. Rev. C **58**, 2459 (1998).
- [4] M. Dugger *et al.* (CLAS Collaboration), Phys. Rev. C **76**, 025211 (2007).
- [5] V. Kubarovsky *et al.* (CLAS Collaboration) Phys. Rev. Lett. **92**, 032001 (2004)
- [6] S. Stepanyan *et al.* (CLAS Collaboration) Phys. Rev. Lett. **91**, 252001 (2003)
- [7] M. Williams *et al.* (CLAS Collaboration) Phys. Rev. C **80**, 045213 (2009)
- [8] M. Dugger *et al.* (CLAS Collaboration) Phys. Rev. Lett. **89**, 222002 (2002)
- [9] I. Horn *et al.* (CB-ELSA Collaboration) Phys. Rev. Lett. **101**, 202002 (2008)
- [10] O. Bartholomy *et al.* (CB-ELSA Collaboration) Phys. Rev. Lett. **94**, 012003 (2005)
- [11] E. F. McNicoll *et al.* (Crystal Ball Collaboration at MAMI) Phys. Rev. C **82**, 035208 (2010)
- [12] H. B. Li *et al.* (BES Collaboration), Nucl. Phys. A **675**, 189C (2000).
- [13] D. M. Asner, T. Barnes, J. M. Bian, I. I. Bigi, N. Brambilla, I. R. Boyko, V. Bytev and K. T. Chao *et al.*, Int. J. Mod. Phys. A **24**, S1 (2009)
- [14] J. Z. Bai *et al.* (BES Collaboration), Phys. Lett. B **510**, 75 (2001).
- [15] R. Koniuk and N. Isgur, Phys. Rev. D **21**, 1868(1980).
- [16] S. Capstick and W. Roberts, Phys. Rev. D **49**, 4570(1994).
- [17] M. Ablikim *et al.* (BES Collaboration) , Phys. Rev. Lett. **97**, 062001(2006).
- [18] M. Ablikim *et al.*(BES Collaboration), Phys. Rev. D **80**, 052004(2009).
- [19] M. Ablikim *et al.* (BES Collaboration), Phys. Rev. D **71**, 072006(2005).
- [20] M. Ablikim *et al.* (BESIII Collaboration) , Phys. Rev. Lett. **110**, 022001 (2013).
- [21] J.P.Alexander, *et al.* (CLEO Collaboration), Phys. Rev. D **82**, 092002(2010).
- [22] M. Ablikim *et al.*(BES Collaboration), Nucl. Instrum. Meth. A **614**, 345(2010).
- [23] Z.Y. Deng *et al.*, HEP&NP. **30**, 371 (2006).
- [24] S. Jadach *et al.*, Phys. Commun. **130**, 260 (2000); Phys. Rev. D **63**, 113009 (2001).
- [25] R.G Ping *et al.*, HEP&NP **32**, 599 (2008).
- [26] K. Nakamura *et al.* (Particle Data Group), J. of Phys. G **37**, 075021 (2010).
- [27] J.C. Chen *et al.*, Phys. Rev. D **62**, 034003 (2000).
- [28] W.D. Li *et al.*, The Offline Software for the BES-III Experiment, Proceeding of CHEP 2006.
- [29] J. X. Wang, Nucl. Instrum. Meth. A **534**, 241 (2004).
- [30] S. N. Dymov, V. S. Kurbatov, I. N. Silin and S. V. Yaschenko, Nucl. Instrum. Meth. A **440**, 431 (2000).
- [31] T. P. Vrana, S. A. Dytman and T. S. H. Lee, Phys. Rept. **328**, 181 (2000).
- [32] M. Ablikim *et al.* (BESIII Collaboration), Phys. Rev. D **83**, 112009 (2011)
- [33] M. Ablikim *et al.* (BESIII Collaboration), Phys. Rev. D **83**, 112005 (2011).
- [34] M. Ablikim *et al.* (BESIII Collaboration), arXiv:1209.6199.
- [35] J. Beringer, *et al.* (Particle Data Group), Phys. Rev. D **86**, 010001 (2012).